



Intermittent Hypoxia and Hypercapnia, a Hallmark of Obstructive Sleep Apnea, Alters the Gut Microbiome and Metabolome

Anupriya Tripathi,^{a,b,c} Alexey V. Melnik,^c Jin Xue,^b Orit Poulsen,^b Michael J. Meehan,^c Gregory Humphrey,^b Lingjing Jiang,^d Gail Ackermann,^b Daniel McDonald,^b Dan Zhou,^b Rob Knight,^{b,e,f} Pieter C. Dorrestein,^{c,f,g} Gabriel G. Haddad^{b,h,i}

^aDivision of Biological Sciences, University of California, San Diego, San Diego, California, USA

^bDepartment of Pediatrics, University of California, San Diego, San Diego, California, USA

^cSkaggs School of Pharmacy and Pharmaceutical Sciences, University of California, San Diego, San Diego, California, USA

^dDepartment of Family Medicine and Public Health, University of California, San Diego, San Diego, California, USA

^eDepartment of Computer Science and Engineering, University of California, San Diego, San Diego, California, USA

^fCenter for Microbiome Innovation, University of California, San Diego, San Diego, California, USA

^gCenter for Computational Mass Spectrometry, University of California, San Diego, San Diego, California, USA

^hDepartment of Neurosciences, University of California, San Diego, San Diego, California, USA

ⁱRady's Children's Hospital, San Diego, California, USA

ABSTRACT Obstructive sleep apnea (OSA) is a common disorder characterized by episodic obstruction to breathing due to upper airway collapse during sleep. Because of the episodic airway obstruction, intermittently low O₂ (hypoxia) and high CO₂ (hypercapnia) ensue. OSA has been associated with adverse cardiovascular and metabolic outcomes, although data regarding potential causal pathways are still evolving. As changes in inspired O₂ and CO₂ can affect the ecology of the gut microbiota and the microbiota has been shown to contribute to various cardiometabolic disorders, we hypothesized that OSA alters the gut ecosystem, which, in turn, exacerbates the downstream physiological consequences. Here, we model human OSA and its cardiovascular consequence using *Ldlr*^{-/-} mice fed a high-fat diet and exposed to intermittent hypoxia and hypercapnia (IHH). The gut microbiome and metabolome were characterized longitudinally (using 16S rRNA amplicon sequencing and untargeted liquid chromatography-tandem mass spectrometry [LC-MS/MS]) and seen to covary during IHH. Joint analysis of microbiome and metabolome data revealed marked compositional changes in both microbial (>10%, most remarkably in *Clostridia*) and molecular (>22%) species in the gut. Moreover, molecules that altered in abundance included microbe-dependent bile acids, enterolignans, and fatty acids, highlighting the impact of IHH on host-commensal organism cometabolism in the gut. Thus, we present the first evidence that IHH perturbs the gut microbiome functionally, setting the stage for understanding its involvement in cardiometabolic disorders.

IMPORTANCE Intestinal dysbiosis mediates various cardiovascular diseases comorbid with OSA. To understand the role of dysbiosis in cardiovascular and metabolic disease caused by OSA, we systematically study the effect of intermittent hypoxic/hypercapnic stress (IHH, mimicking OSA) on gut microbes in an animal model. We take advantage of a longitudinal study design and paired omics to investigate the microbial and molecular dynamics in the gut to ascertain the contribution of microbes on intestinal metabolism in IHH. We observe microbe-dependent changes in the gut metabolome that will guide future research on unrecognized mechanistic links be-


Received 15 February 2018 Accepted 8 May 2018 Published 5 June 2018

Citation Tripathi A, Melnik AV, Xue J, Poulsen O, Meehan MJ, Humphrey G, Jiang L, Ackermann G, McDonald D, Zhou D, Knight R, Dorrestein PC, Haddad GG. 2018. Intermittent hypoxia and hypercapnia, a hallmark of obstructive sleep apnea, alters the gut microbiome and metabolome. *mSystems* 3: e00020-18. <https://doi.org/10.1128/mSystems.00020-18>.

Editor Janet K. Jansson, Pacific Northwest National Laboratory

Copyright © 2018 Tripathi et al. This is an open-access article distributed under the terms of the [Creative Commons Attribution 4.0 International license](https://creativecommons.org/licenses/by/4.0/).

Address correspondence to Rob Knight, rknight@ucsd.edu, Pieter C. Dorrestein, pdorrestein@ucsd.edu, or Gabriel G. Haddad, ghaddad@ucsd.edu.

 Significant perturbations in gut microbiota and microbial metabolites due to low inspired oxygen and high carbon dioxide in sleep apnea may explain the high incidence of cardiovascular disease in sleep apnea patients.

tween gut microbes and comorbidities of OSA. Additionally, we highlight novel and noninvasive biomarkers for OSA-linked cardiovascular and metabolic disorders.

KEYWORDS cardiovascular, metabolism, microbiome, sleep apnea

Obstructive sleep apnea (OSA) afflicts nearly 12% of the adult population in the United States, with an annual cost burden of nearly \$149.6 billion, per a recent study commissioned by the American Academy of Sleep Medicine (1). Timely diagnosis and treatment of OSA improves not only sleep and cognitive function but also management of comorbid cardiometabolic diseases (CMDs). Therefore, identifying the mechanisms underlying the downstream consequences of OSA would aid in development of effective treatment modalities, reducing overall health care utilization.

OSA is marked by changes in oxygen and carbon dioxide-inspired concentrations, which impact the gut microbial community (2). Since the gut microbiota plays a key role in the metabolism of dietary precursors, including lipids, cholesterol, and choline, it impacts the cardiometabolic health of the host (3). Gut dysbiosis has already been linked to an array of cardiovascular and metabolic disorders, such as hypertension, type 2 diabetes, hepatic steatosis, and atherosclerosis (4, 5). Additionally, previous work has identified specific gut bacteria to be significantly correlated with plasma cholesterol and apolipoprotein levels (6). Thus, probing this commensal ecosystem may provide a valuable avenue of investigation to understand the mechanisms underlying the cardiovascular consequences of OSA. In this study, we investigated the taxonomic and molecular alterations in the gut microbiome that potentially mediate the interplay between OSA and related CMDs.

We used atherosclerosis-prone (*Ldlr*^{-/-}) adult mice fed a high-fat diet (HFD) enriched in cholesterol and milk fat (resembling Western dietary practices) to evaluate atherosclerosis risk in OSA. We previously demonstrated that IHH increases atherosclerosis plaque formation in this model (7). As episodic hypoxia and hypercapnia mimic the changes in blood gases that occur in OSA-driven downstream consequences (8), these mice were exposed to IHH (treatment group; $n = 8$) or air (control group; $n = 8$) and examined longitudinally for 6 weeks (see Fig. S1 in the supplemental material). Fecal samples, representative of the gut ecosystem, were collected at baseline and twice each week thereafter, and the microbiome and metabolome were profiled using 16S rRNA amplicon sequencing and liquid chromatography-tandem mass spectrometry (LC-MS/MS)-based untargeted mass spectrometry, respectively. These data were processed to obtain relative abundances of microbial and molecular species per sample (referred to as “feature tables” henceforth), which were used for comparing mice mimicking humans with OSA and control mice.

First, we performed principal-coordinate analysis (PCoA) on the microbiome and metabolome feature tables to identify major factors driving the clustering of samples. Figure 1 shows the PCoA results plotted against time to visualize the dynamics of clustering based on the gut microbiome (unweighted UniFrac distances [9] are shown in Fig. 1a) and the metabolome (Gower distances [10] are shown in Fig. 1b and c) as the duration of IHH exposure increases. Here, the first fecal sample represents the baseline gut composition before animals were switched to an HFD. There is a rapid shift in both microbial and molecular composition due to HFD alone, consistent with similar previous findings (11–13). Moreover, starting from a highly congruent gut composition, IHH-exposed mice significantly diverge from controls with increasing exposure duration (a permutational multivariate analysis of variance [PERMANOVA] test was performed per time point [Table S1]). This demonstrates that prolonged IHH exposure (analogous to chronic OSA) cumulatively perturbs the gut microbiome and metabolome. We tested the relationship between the two omics data sets by superimposing the principal coordinates computed from microbiome and metabolome data (procrustes analysis [14]) (Fig. 1d and e). The ordination spaces are correlated (Mantel test r statistic = 0.36, $P < 0.001$), and changes in the metabolome and microbiome of samples within the

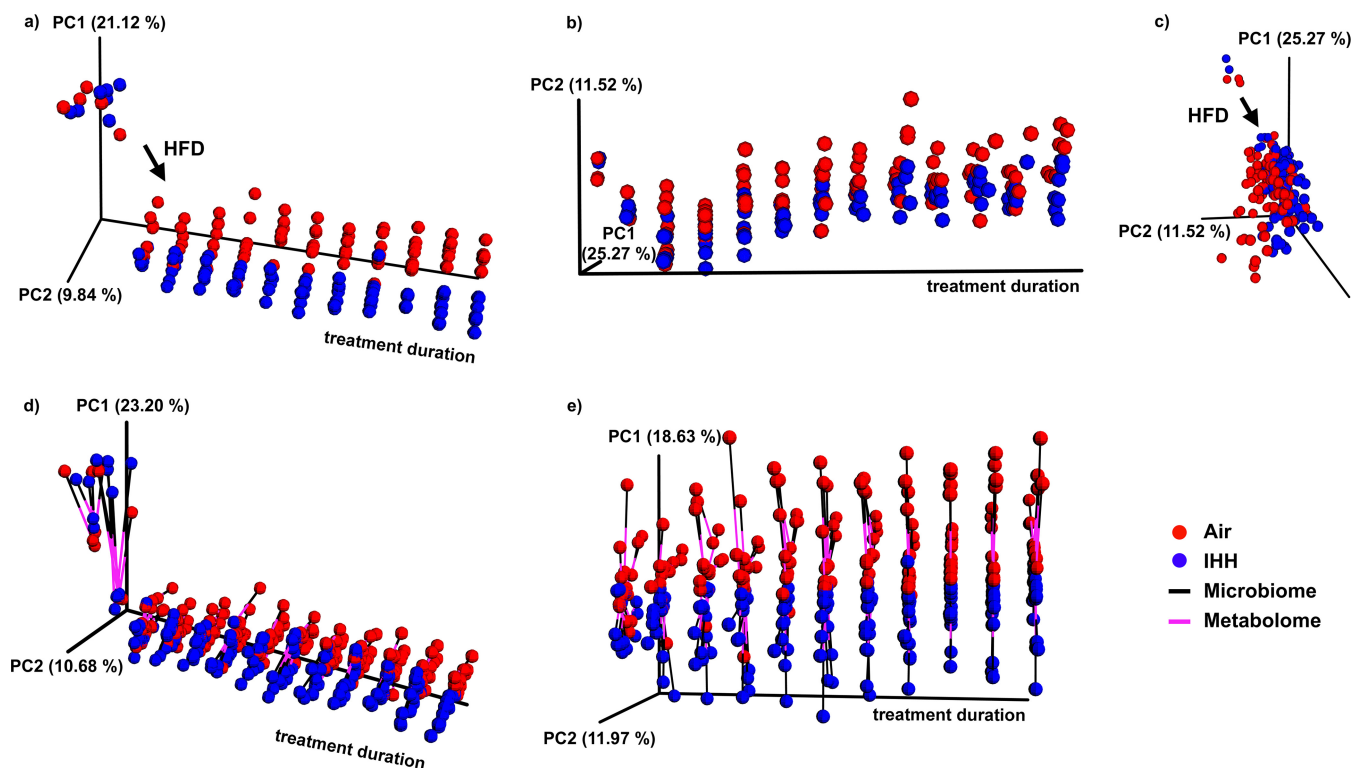


FIG 1 Principal-coordinate analysis (PCoA) and procrustes analysis of the gut microbiome and metabolome. (a) PCoA of the microbiome (16S rRNA sequencing) data using unweighted UniFrac distances; (b and c) PCoA of the metabolome (untargeted LC-MS/MS) data using Gower distances; (d and e) procrustes analysis of the microbiome and metabolome data sets with (d) and without (e) baseline samples. The duration of treatment (in weeks, with an interval length of 0.5 week) is constrained to be one of the axes in the ordination plots (a to e). In the procrustes analysis (d and e), the coordinates for a sample obtained using microbiome data (black lines) are connected to coordinates for the same sample obtained using metabolome data (pink lines). This analysis stretches, rotates, and superimposes ordinations generated from one data set over the other, while preserving distances within each individual matrix. The goal is to find the best fit between two matrices to infer whether one data set coherently captures the properties of the other. PC1, principal component 1; HFD, high-fat diet; IHH, intermittent hypoxia and hypercapnia.

treatment groups over time are proportional, suggesting microbe-dependent changes in intestinal metabolism with chronic OSA.

We then tested for specific microbes and metabolites that changed with OSA. More than 80 (of ~730) microbial features differed significantly between the IHH-exposed group and controls (by permutation test with discrete false-discovery rate [FDR] correction [15]). Figure S2a presents a global overview of these changes in gut microbiota per sample (sorted by duration of treatment). Table S2 provides a list of these differentially represented bacteria that potentially contribute to alterations in gut metabolism due to IHH. Figure 2a to f display trends in relative abundances of bacteria showing the largest differences, which belong to the *Mogibacteriaceae* (family), *Oscillospira* (genus), *Lachnospiraceae* (family), and *Clostridiaceae* (family). Previous studies have consistently associated these taxonomic groups with metabolic and inflammatory disturbances in the host (16, 17), which suggests that related mechanisms might be at play in driving the consequences of hypoxic and hypercapnic stress.

Using the same statistical approach, we found that more than 380 out of ~1,700 molecular species (MS1 spectral features) differed significantly in relative abundance in animals exposed to IHH. Figure S2b provides a global representation of these differentially abundant molecules in samples belonging to treatment and control groups and sorted by treatment duration (Table S3 provides a comprehensive list of these molecules). To gain insight into the structures of these differentially abundant metabolites, we performed molecular networking using Global Natural Products Social Molecular Networking (GNPS) (18). The molecular network is constructed using a cosine similarity measure between tandem mass spectral data and then visualized using cytoscape (19)

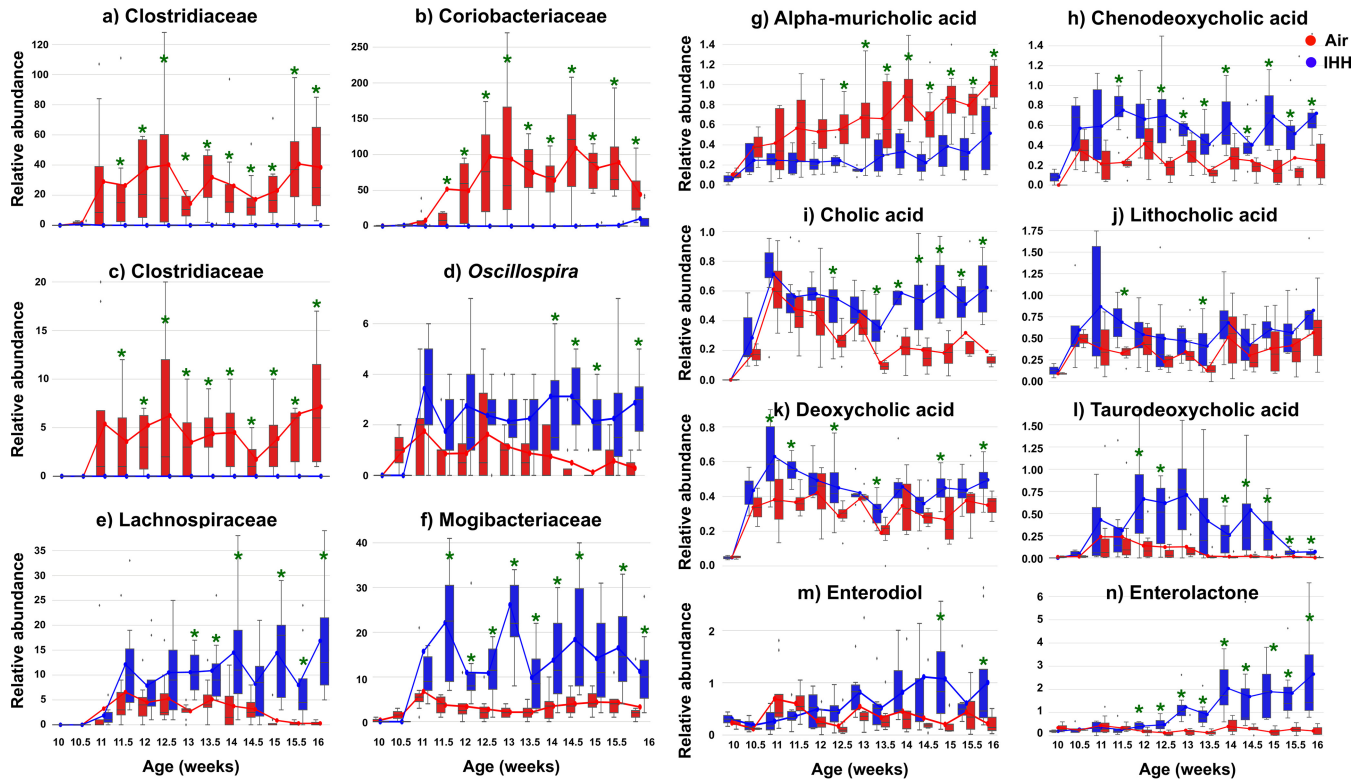


FIG 2 Changes in the gut microbes and molecules due to IHH exposure. (a to f) Top differentially abundant sOTUs elevated in the control group (a, b, and c) and treatment group (d, e, and f). The sOTUs belonging to the families *Clostridiaceae* (a and c) and *Coriobacteriaceae* (b) were elevated in controls, whereas those belonging to the genus *Oscillospira* (d) and the families *Lachnospiraceae* (e) and *Mogibacteriaceae* (f) were higher in IHH-exposed mice than in control mice. (g to n) Trends in abundances of significantly differential primary bile acids alpha-muricholic acid (g), chenodeoxycholic acid (h), and cholic acid (i), the secondary bile acids lithocholic acid (j) and deoxycholic acid (k), and the conjugated secondary bile acid taurodeoxycholic acid (l). (m and n) Trends in abundances of the significantly differential xenoestrogens enterodiol (m) and enterolactone (n). Significantly differential time points are denoted by asterisks. IHH, intermittent hypoxia and hypercapnia.

(Fig. S3). Each node in the network, which represents a consensus MS/MS spectrum, was searched against public libraries in this study. In total, we annotated about 400 molecular compounds in the GNPS database, including bile acids (BAs), fatty acids, and phytoestrogens. Additionally, all key compounds discussed in this work were defined to the highest level of annotation per the metabolomic standards initiative using commercial standards (Fig. S4, Fig. S5, and Table S4) (20).

Interestingly, the top differentially abundant features detected between IHH and control mice included molecules known to depend on gut microbes for their production. Below, we discuss some of these metabolites and their implications with respect to consequences of OSA.

Alterations in bile acids. We observed significant alterations in BAs between IHH-exposed mice and control groups (Table S3). Figure 2g to n display these trends in primary (Fig. 2g to i) and secondary (Fig. 2j to l) bile acids with increasing IHH exposure duration. Primary BAs are amphipathic molecules synthesized in the liver from cholesterol. These are conjugated to glycine or taurine and released in the biliary tract. Together with other biliary components, these facilitate the emulsification and transportation of dietary fats, cholesterol, and fat-soluble vitamins. About 95% of the BAs are reabsorbed in the terminal ileum and recycled. The remaining 5% reach the colon and are deconjugated, dehydrogenated, and dehydroxylated by the intestinal bacteria to form secondary BAs (21). BAs, including microbially generated BAs, are potent signaling molecules that interact with the farnesoid X receptor (FXR) (expressed in the liver and intestine), which modulates BA synthesis by the liver (22). Perturbations in the gut microbial population disrupt normal signaling properties that regulate BA production and can profoundly alter the BA composition in the gut. A range of diseases, including

cardiometabolic diseases, are characterized by aberrant BA profiles (23), and prolonged perturbations in the BA pool might also be a factor in mediating the consequences of OSA.

Elevations in phytoestrogens. The dietary hormones enterolactone (mammalian lignan) and enterodiol (oxidation product of enterolactone) were significantly elevated in the exposed mice compared to their levels in controls. Figure 2m and n show the trends in their abundances with increasing duration of IHH exposure. These molecules are phytoestrogens, i.e., plant-derived hormones that structurally mimic estrogen and are produced by intestinal microbiota upon bioconversion of dietary lignans. Owing to their affinity to estrogen receptors (producing estrogenic or/and antiestrogenic effects [24]), they perturb many hormone-dependent systems in the body and have been linked to adverse metabolic, reproductive, and neurological outcomes (25). Sex-specific differences in OSA-diagnostic symptoms and risk factors suggest hormonal involvement (26, 27). However, the contribution of microbes in maintaining hormonal homeostasis has not yet been investigated. Therefore, these findings motivate novel avenues of research for biomarkers and therapeutic targets to manage the metabolic consequences of OSA.

Alterations in fatty acids. In addition to detecting changes in bile acids and phytoestrogens, we detected differentially abundant fatty acid-related chemical families (Table S3). For example, we noted a significant reduction in a molecular feature matched to elaidic acid. Elaidic acid is an unsaturated fatty acid that increases plasma cholesteryl ester transfer protein (CETP) activity, which modulates systemic levels of low-density lipoprotein (LDL) and high-density lipoprotein (HDL) cholesterol. A decrease in elaidic acid in the IHH-exposed group suggests reduction in plasma CETP activity, a mechanism associated with adverse cardiovascular effects (28). Similarly, phytomonic, jasmonic, hexadecanoic, linoleic, and conjugated linoleic acids were also reduced in exposed mice compared to levels in controls. Of these, phytomonic acid and conjugated linoleic acid are known to be microbially produced (29, 30), suggesting that changes in the microbiome contribute to these changes in metabolome.

In summary, we demonstrate that IHH, a hallmark of OSA, changes the microbiota and the chemistry in the gut. We have highlighted changes in bile acids, phytoestrogens, and fatty acids under OSA-related conditions that could lead to CMDs. The present results reveal a previously unrecognized mechanistic link between OSA and gut microbes. It suggests that targeting gut microbiota and their metabolites may serve as a potential therapeutic approach for the treatment of cardiometabolic consequences of OSA patients.

Animals. Atherosclerosis-prone 10-week-old male *Ldlr*^{-/-} mice in the C57BL/6J background (stock number 002207; The Jackson Laboratory, Bar Harbor, ME) were used in this study (31). *Ldlr* deficiency was confirmed by PCR per the vendor's instructions. All animal protocols were approved by the Animal Care Committee of the University of California, San Diego, and followed the Guide for the Care and Use of Laboratory Animals of the National Institutes of Health (32).

High-fat diet treatment. Starting at 10 weeks of age, male mice were provided with a high-fat diet (HFD) containing 1.25% cholesterol and 21% milk fat (4.5 kcal/g; TD96121; Harlan-Teklad, Madison, WI) for 6 weeks while being exposed to either IHH or room air.

IHH exposure. Intermittent hypoxia and hypercapnia (IHH) was maintained in a computer-controlled atmosphere chamber system (OxyCycler; Reming Bioinstruments, Redfield, NY) as previously described (7). IHH exposure was introduced to the mice in short periods (~4 min) of synchronized reduction of O₂ (from 21% to 8%) and elevation of CO₂ (from ~0.5% to 8%), separated by alternating periods (~4 min) of normoxia ([O₂] = 21%) and normocapnia ([CO₂] = ~0.5%), with 1- to 2-min ramp intervals for 10 h per day during the light cycle for 6 weeks. This treatment protocol mimics the severe clinical condition observed in obstructive sleep apnea patients. Mice on the same HFD but in room air were used as controls.

As the experimental setup requires IHH-exposed mice in a controlled atmosphere chamber and controls in room air, we ensured that the effect of treatment is not confounded by the effect of distinct housing conditions. To do so, we used two cages per treatment group, and we compared the relative effect sizes of treatments and cages with redundancy analysis (RDA), which estimates the independent effect size of each covariate on microbiome composition variation based on unweighted UniFrac distance (33). The RDA results showed that treatment had a higher effect size than the cages, more specifically, that treatment contributed to 11.6% of the microbiome community variation, while cages had an independent effect size of around 9.8%; with respect to the metabolome, treatment contributed to 6.2% of the variation, while cages contributed to only about 0.7% of the variation.

LC-MS/MS data acquisition. Prior to LC-MS/MS analysis, fecal samples were prepared using the following extraction procedures. For extraction, 500 μ l of 50:50 methanol-H₂O was added to all fecal samples (30 to 50 mg approximately) and vortexed. Fecal pellets in extraction solvent were placed in an ultrasonic bath and sonicated for 30 min to break apart the pellet and then allowed to incubate for an additional 30 min. Extracted samples were then centrifuged to separate insoluble material, and 450 μ l of each liquid extract was subsequently transferred to a 96-well deep-well plate and dried completely using centrifugal evaporation (CentriVap centrifugal vacuum concentrator; Labconco, Kansas City, MO). The dried extracts were resuspended in 150 μ l of methanol-H₂O (1:1, vol/vol), with 1 μ M amitriptyline included as an autosampler injection standard. After resuspension, the samples were transferred into 96-well plates and analyzed on a Vanquish ultrahigh-performance liquid chromatography (UPLC) system coupled to a Q Exactive orbital ion trap (Thermo Fisher Scientific, Bremen, Germany). For the chromatographic separation, a C₁₈ core shell column (Kinetex column, 50 by 2 mm, 1.7- μ m particle size, 100-Å pore size; Phenomenex, Torrance, CA) with a flow rate of 0.5 ml/min (solvent A, H₂O-0.1% formic acid [FA]; solvent B, acetonitrile-0.1% FA) was used. After being injected, the samples were eluted from 0 to 0.5 min with a linear gradient of 5% solvent B, from 0.5 to 4 min with 5 to 50% solvent B, and from 4 to 5 min with 50 to 99% solvent B, followed by a 2-min washout phase at 99% solvent B and a 2-min reequilibration phase at 5% solvent B. For online MS/MS measurements, the flow was directed to a heated electrospray ionization (HESI) source. The ESI parameters were set to 35 liters/min for the sheath gas flow, 10 liter/min for the auxiliary gas flow, 2 liters/min for the sweep gas flow, and 400°C for the auxiliary gas temperature. The spray voltage was set to 3.5 kV, and the inlet capillary was set to 250°C. A 50-V S-lens radio frequency (RF) level was applied. Product ion spectra were recorded in data-dependent acquisition (DDA) mode. Both MS1 survey scans (m/z 150 to 1,500) and up to 5 MS/MS scans of the most abundant ions per duty cycle were measured with a resolution (R) of 17,500 with 1 microscan in positive mode. The maximum ion injection time was set to 100 ms. MS/MS precursor selection windows were set to m/z 3 with an m/z 0.5 offset. Normalized collision energy was stepwise increased from 20 to 30 to 40% with a z of 2 as the default charge state. MS/MS experiments were automatically triggered at the apex of a peak within 2 to 15 s from their first occurrence. Dynamic exclusion was set to 5 s.

LC-MS/MS data analysis. Feature detection was as follows. Thermo raw data sets were converted to m/z extensible markup language (mzXML) in centroid mode using MSConvert (part of ProteoWizard) (34, 35). All mzXML files were cropped with an m/z range of 75.00 to 1,000.00 Da. MS1-based feature detection and MS2-based molecular networking was performed using the GNPS workflow (<https://gnps.ucsd.edu/ProteoSAFe/static/gnps-splash.jsp>) (18). The parameters used are detailed at the following URL: <http://gnps.ucsd.edu/ProteoSAFe/status.jsp?task=c6438af750784d919dcd0ee0a783b4fc>. Feature extraction parameters were optimized using MZmine2 (<http://mzmine.sourceforge.net/>) (36) with a signal threshold of 2.0e5 and a 0.3-s minimum peak width. The mass tolerance was set to 10 ppm, and the maximum allowed retention time deviation was set to 10 s. For chromatographic deconvolution, the local minimum search algorithm

was used with a minimum relative peak height of 1% and a minimum retention time range of 0.6 s. The maximum peak width was set to 1 min. After isotope peak removal, the peak lists of all samples were aligned with the above-mentioned retention time and mass tolerances. After the creation of a feature matrix containing the feature retention times and the exact mass and peak areas of the corresponding extracted ion chromatograms, the metadata of the samples (treatment type and duration) were added. The signal intensities of the features were normalized (probabilistic quotient normalization [PQN]) (37) to an internal standard (m/z 278.189; real time, 3.81 min) for subsequent analysis.

MS/MS annotations were as follows. Molecular features, in the form of MS/MS spectra, were putatively identified using MS2-based spectral library matches. The false-discovery rate (FDR) was estimated using a decoy database approach (38) in GNPS and was found to be less than 1% above a cosine similarity score of 0.6 (GNPS job link, <https://gnps.ucsd.edu/ProteoSAFe/status.jsp?task=feac48de4c9f45d485403e3feb7a470d>). Therefore, we used a cosine score of 0.65 here. For level 1 annotation, as defined by the 2007 metabolomics standards initiative for differentially abundant metabolites, we purchased authentic standards of alpha-muricholic acid, chenodeoxycholic acid, cholic acid, lithocholic acid, deoxycholic acid, taurodeoxycholic acid, and the xenoestrogens enterodiol and enterolactone from Cayman Chemical (Ann Arbor, MI) and analyzed them using the same LC-MS/MS method described above. We then compared and verified the exact masses, fragmentation patterns, and retention times of those compounds to ensure correct annotations (Fig. S2 and Fig. S3).

Statistical analysis was carried out as follows. QIIME 1.9.1 was used to perform principal-coordinate analysis (PCoA) (`beta_diversity.py`, a Gower dissimilarity metric [10]) and a PERMANOVA test (`compare_categories.py`). The PCoA plots were visualized in EMPeror (39). Differential abundance analysis was performed using discrete FDRs (15).

16S rRNA sequencing. DNA extraction and 16S rRNA amplicon sequencing were done using Earth Microbiome Project (EMP) standard protocols (<http://www.earthmicrobiome.org/protocols-and-standards/16s>) (40). In brief, DNA was extracted using the MO BIO PowerSoil DNA extraction kit (Carlsbad, CA). Amplicon PCR was performed on the V4 region of the 16S rRNA gene using the primer pair 515f to 806r with Golay error-correcting barcodes on the reverse primer. Amplicons were barcoded and pooled in equal concentrations for sequencing. The amplicon pool was purified with the MO BIO UltraClean PCR cleanup kit and sequenced on the Illumina HiSeq 2500 sequencing platform. Sequence data were demultiplexed and minimally quality filtered using the QIIME 1.9.1 script `split_libraries_fastq.py`, with a Phred quality threshold of 3 and default parameters to generate per-study FASTA sequence files.

16S marker gene data analysis. Feature detection and identification were performed as follows. The raw sequence data were processed using the Deblur workflow (41) with default parameters in Qiita (<https://qiita.ucsd.edu/>). This generated a sub-operational taxonomic unit (sOTU) abundance per sample (BIOM format) (41, 42). Taxonomies for sOTUs were assigned using the sklearn-based taxonomy classifier (feature classifier plug-in) in QIIME 2 (43). The sOTU table was rarefied to a depth of 2,000 sequences/sample to control for sequencing effort (44). A phylogeny was inferred using SATé-enabled phylogenetic placement (45), which was used to insert 16S Deblur sOTUs into Greengenes 13_8 at a 99% phylogeny.

For statistical analysis, QIIME 2 was used to perform PCoA (unweighted UniFrac distances [9]). QIIME 1.9.1 was used for the PERMANOVA test (`compare_categories.py`), Mantel test (`compare_distance_matrices.py`), and procrustes analysis (`transform_coordinate_matrices.py`). The PCoA and procrustes plots were visualized in EMPeror. (39) Differential-abundance analysis was performed using discrete FDRs (15).

Data availability. The data generated in this study are available publicly under the following accession numbers: for metabolomics data, [MSV000081482](https://doi.org/10.26434/chemrxiv-2018-05-01); for commercial standards, [MSV000081853](https://doi.org/10.26434/chemrxiv-2018-05-01); and for microbiome data, [ERP106495](https://doi.org/10.26434/chemrxiv-2018-05-01) (EBI database). Data

analysis has been documented in Jupyter notebooks available on GitHub (https://github.com/knightlab-analyses/haddad_osa).

SUPPLEMENTAL MATERIAL

Supplemental material for this article may be found at <https://doi.org/10.1128/mSystems.00020-18>.

FIG S1, TIF file, 0.3 MB.

FIG S2, EPS file, 0.3 MB.

FIG S3, TIF file, 1.3 MB.

FIG S4, TIF file, 0.2 MB.

FIG S5, TIF file, 0.2 MB.

TABLE S1, PDF file, 0.05 MB.

TABLE S2, XLS file, 0.1 MB.

TABLE S3, XLS file, 0.1 MB.

TABLE S4, PDF file, 0.05 MB.

ACKNOWLEDGMENTS

We acknowledge NIH grants GMS10RR029121 and 5P41GM103484-07 for the shared instrumentation infrastructure that enabled this work.

A.T. wrote the initial manuscript and managed, analyzed, and interpreted the data. A.V.M. contributed to the manuscript and analyzed and interpreted the data. J.X. contributed to the manuscript and the study design. O.P. contributed to the study design and collected samples for analysis. M.J.M. and G.H. performed mass spectrometry and amplicon sequencing, respectively. L.J. analyzed and interpreted the data. G.A. curated the metadata. D.M. contributed to the manuscript and interpreted the data. D.Z. contributed to the study design. R.K., P.C.D., and G.G.H. conceived and designed the study, interpreted the data, and contributed to the manuscript. All authors worked together to finalize and approve the manuscript.

REFERENCES

- Watson NF. 2016. Health care savings: the economic value of diagnostic and therapeutic care for obstructive sleep apnea. *J Clin Sleep Med* 12:1075–1077. <https://doi.org/10.5664/jcsm.6034>.
- Moreno-Indias I, Torres M, Montserrat JM, Sanchez-Alcoholado L, Cardona F, Tinahones FJ, Gozal D, Poroyko VA, Navajas D, Queipo-Ortuño MI, Farré R. 2015. Intermittent hypoxia alters gut microbiota diversity in a mouse model of sleep apnoea. *Eur Respir J* 45:1055–1065. <https://doi.org/10.1183/09031936.00184314>.
- García-Ríos A, Torres-Peña JD, Pérez-Jiménez F, Pérez-Martínez P. 2017. Gut microbiota: a new marker of cardiovascular disease. *Curr Pharm Des* 23:3233–3238. <https://doi.org/10.2174/1381612823666170317144853>.
- He M, Shi B. 2017. Gut microbiota as a potential target of metabolic syndrome: the role of probiotics and prebiotics. *Cell Biosci* 7:54. <https://doi.org/10.1186/s13578-017-0183-1>.
- Okubo H, Nakatsu Y, Kushiya A, Yamamotoya T, Matsunaga Y, Inoue MK, Fujishiro M, Sakoda H, Ohno H, Yoneda M, Ono H, Asano T. 2018. Gut microbiota as a therapeutic target for metabolic disorders. *Curr Med Chem* 25:984–1001. <https://doi.org/10.2174/0929867324666171009121702>.
- Koren O, Spor A, Felin J, Fåk F, Stombaugh J, Tremaroli V, Behre CJ, Knight R, Fagerberg B, Ley RE, Bäckhed F. 2011. Human oral, gut, and plaque microbiota accelerate atherosclerosis, partially via trimethylamine-oxide. *Am J Respir Cell Mol Biol* 57:581–588. <https://doi.org/10.1165/rcmb.2017-0086OC>.
- Sforza E, Roche F. 2016. Chronic intermittent hypoxia and obstructive sleep apnea: an experimental and clinical approach. *Hypoxia* 4:99–108. <https://doi.org/10.2147/HP.S103091>.
- Lozupone C, Knight R. 2005. UniFrac: a new phylogenetic method for comparing microbial communities. *Appl Environ Microbiol* 71:8228–8235. <https://doi.org/10.1128/AEM.71.12.8228-8235.2005>.
- Gower JC. 1971. A general coefficient of similarity and some of its properties. *Biometrics* 27:857. <https://doi.org/10.2307/2528823>.
- David LA, Maurice CF, Carmody RN, Gootenberg DB, Button JE, Wolfe BE, Ling AV, Devlin AS, Varma Y, Fischbach MA, Biddinger SB, Dutton RJ, Turnbaugh PJ. 2014. Diet rapidly and reproducibly alters the human gut microbiome. *Nature* 505:559–563. <https://doi.org/10.1038/nature12820>.
- Esko T, Hirschhorn JN, Feldman HA, Hsu Y-HH, Deik AA, Clish CB, Ebbeling CB, Ludwig DS. 2017. Metabolomic profiles as reliable biomarkers of dietary composition. *Am J Clin Nutr* 105:547–554. <https://doi.org/10.3945/ajcn.116.144428>.
- Turnbaugh PJ, Ridaura VK, Faith JJ, Rey FE, Knight R, Gordon JL. 2009. The effect of diet on the human gut microbiome: a metagenomic analysis in humanized gnotobiotic mice. *Sci Transl Med* 1:6ra14. <https://doi.org/10.1126/scitranslmed.3000322>.
- Gower JC. 1975. Generalized procrustes analysis. *Psychometrika* 40:33–51. <https://doi.org/10.1007/BF02291478>.
- Jiang L, Amir A, Morton JT, Heller R, Arias-Castro E, Knight R. 2017. Discrete false-discovery rate improves identification of differentially abundant microbes. *mSystems* 2:e00092-17. <https://doi.org/10.1128/mSystems.00092-17>.
- Pascal V, Pozuelo M, Borrueal N, Casellas F, Campos D, Santiago A, Martínez X, Varela E, Sarrabayrouse G, Machiels K, Vermeire S, Sokol H, Guarner F, Manichanh C. 2017. A microbial signature for Crohn's disease. *Gut* 66:813–822. <https://doi.org/10.1136/gutjnl-2016-313235>.
- Kameyama K, Itoh K. 2014. Intestinal colonization by a Lachnospiraceae bacterium contributes to the development of diabetes in obese mice. *Microbes Environ* 29:427–430. <https://doi.org/10.1264/jjme2.ME14054>.
- Wang M, Carver JJ, Phelan VV, Sanchez LM, Garg N, Peng Y, Nguyen DD, Watrous J, Kapono CA, Luzzatto-Knaan T, Porto C, Bouslimani A, Melnik AV, Meehan MJ, Liu W-T, Crüsemann M, Boudreau PD, Esquenazi E, Sandoval-Calderón M, Kersten RD, Pace LA, Quinn RA, Duncan KR, Hsu C-C, Floros DJ, Gavilan RG, Kleigrewe K, Northen T, Dutton RJ, Parrot D, Carlson EE, Aigle B, Michelsen CF, Jelsbak L, Sohlenkamp C, Pevzner P,

- Edlund A, McLean J, Piel J, Murphy BT, Gerwick L, Liaw C-C, Yang Y-L, Humpf H-U, Maansson M, Keyzers RA, Sims AC, Johnson AR, Sidebottom AM, Sedio BE, et al. 2016. Sharing and community curation of mass spectrometry data with Global Natural Products Social Molecular Networking. *Nat Biotechnol* 34:828–837. <https://doi.org/10.1038/nbt.3597>.
19. Shannon P, Markiel A, Ozier O, Baliga NS, Wang JT, Ramage D, Amin N, Schwikowski B, Ideker T. 2003. Cytoscape: a software environment for integrated models of biomolecular interaction networks. *Genome Res* 13:2498–2504. <https://doi.org/10.1101/gr.1239303>.
 20. Sumner LW, Amberg A, Barrett D, Beale MH, Beger R, Daykin CA, Fan TW-M, Fiehn O, Goodacre R, Griffin JL, Hankemeier T, Hardy N, Harnly J, Higashi R, Kopka J, Lane AN, Lindon JC, Marriott P, Nicholls AW, Reilly MD, Thaden JJ, Viant MR. 2007. Proposed minimum reporting standards for chemical analysis Chemical Analysis Working Group (CAWG) Metabolomics Standards Initiative (MSI). *Metabolomics* 3:211–221. <https://doi.org/10.1007/s11306-007-0082-2>.
 21. Chiang JYL. 2013. Bile acid metabolism and signaling. *Compr Physiol* 3:1191–1212. <https://doi.org/10.1002/cphy.c120023>.
 22. Ramírez-Pérez O, Cruz-Ramón V, Chinchilla-López P, Méndez-Sánchez N. 2017. The role of the gut microbiota in bile acid metabolism. *Ann Hepatol* 16:s15–s20. <https://doi.org/10.5604/01.3001.0010.5494>.
 23. Joyce SA, Gahan CGM. 2017. Disease-associated changes in bile acid profiles and links to altered gut microbiota. *Dig Dis* 35:169–177. <https://doi.org/10.1159/000450907>.
 24. Patisaul HB, Jefferson W. 2010. The pros and cons of phytoestrogens. *Front Neuroendocrinol* 31:400–419. <https://doi.org/10.1016/j.yfme.2010.03.003>.
 25. Gore AC, Chappell VA, Fenton SE, Flaws JA, Nadal A, Prins GS, Toppari J, Zoeller RT. 2015. Executive summary to EDC-2: the Endocrine Society's second scientific statement on endocrine-disrupting chemicals. *Endocr Rev* 36:593–602. <https://doi.org/10.1210/er.2015-1093>.
 26. McKinney J, Ortiz-Young D, Jefferson F. 2015. Gender differences in obstructive sleep apnea and the associated public health burden. *Sleep Biol Rhythms* 13:196–209. <https://doi.org/10.1111/sbr.12107>.
 27. Jehan S, Auguste E, Zizi F, Pandi-Perumal SR, Gupta R, Attarian H, Jean-Louis G, McFarlane SI. 2016. Obstructive sleep apnea: women's perspective. *J Sleep Med Disord* 3:1064.
 28. Abbey M, Nestel PJ. 1994. Plasma cholesteryl ester transfer protein activity is increased when trans-elaidic acid is substituted for cis-oleic acid in the diet. *Atherosclerosis* 106:99–107. [https://doi.org/10.1016/0021-9150\(94\)90086-8](https://doi.org/10.1016/0021-9150(94)90086-8).
 29. Hofmann K, Tausig F. 1955. On the identity of phytomonic and lactobacillic acids; a reinvestigation of the fatty acid spectrum of *Agrobacterium* (*Phytomonas*) *tumefaciens*. *J Biol Chem* 213:425–432.
 30. Van Nieuwenhove CP, Teran V, Nelina S. 2012. Conjugated linoleic and linolenic acid production by bacteria: development of functional foods, p 55–80. *In* Rigobelo E (ed), *Probiotics*. IntechOpen <https://www.intechopen.com/books/probiotics/conjugated-linoleic-and-linolenic-acid-production-by-bacteria-development-of-functional-foods>.
 31. Ishibashi S, Brown MS, Goldstein JL, Gerard RD, Hammer RE, Herz J. 1993. Hypercholesterolemia in low density lipoprotein receptor knockout mice and its reversal by adenovirus-mediated gene delivery. *J Clin Invest* 92:883–893. <https://doi.org/10.1172/JCI116663>.
 32. National Research Council. 2011. *Guide for the care and use of laboratory animals*, 8th ed. National Academies Press, Washington, DC.
 33. Falony G, Joossens M, Vieira-Silva S, Wang J, Darzi Y, Faust K, Kurilshikov A, Bonder MJ, Valles-Colomer M, Vandeputte D, Tito RY, Chaffron S, Rymenans L, Verspecht C, De Sutter L, Lima-Mendez G, D'hoel K, Jonckheere K, Homola D, Garcia R, Tigchelaar EF, Eeckhaut L, Fu J, Henckaerts L, Zhernakova A, Wijmenga C, Raes J. 2016. Population-level analysis of gut microbiome variation. *Science* 352:560–564. <https://doi.org/10.1126/science.aad3503>.
 34. Adusumilli R, Mallick P. 2017. Data conversion with ProteoWizard msConvert. *Methods Mol Biol* 1550:339–368. https://doi.org/10.1007/978-1-4939-6747-6_23.
 35. Kessner D, Chambers M, Burke R, Agus D, Mallick P. 2008. ProteoWizard: open source software for rapid proteomics tools development. *Bioinformatics* 24:2534–2536. <https://doi.org/10.1093/bioinformatics/btn323>.
 36. Pluskal T, Castillo S, Villar-Briones A, Oresic M. 2010. MZmine 2: modular framework for processing, visualizing, and analyzing mass spectrometry-based molecular profile data. *BMC Bioinformatics* 11:395. <https://doi.org/10.1186/1471-2105-11-395>.
 37. Dieterle F, Ross A, Schlotterbeck G, Senn H. 2006. Probabilistic quotient normalization as robust method to account for dilution of complex biological mixtures. Application in 1H NMR metabolomics. *Anal Chem* 78:4281–4290. <https://doi.org/10.1021/ac051632c>.
 38. Scheubert K, Hufsky F, Petras D, Wang M, Nothias LF, Dührkop K, Bandeira N, Dorrestein PC, Böcker S. 2017. Significance estimation for large scale metabolomics annotations by spectral matching. *Nat Commun* 8:1494. <https://doi.org/10.1038/s41467-017-01318-5>.
 39. Vázquez-Baeza Y, Pirrung M, Gonzalez A, Knight R. 2013. EMPERor: a tool for visualizing high-throughput microbial community data. *Gigascience* 2:16. <https://doi.org/10.1186/2047-217X-2-16>.
 40. Caporaso JG, Lauber CL, Walters WA, Berg-Lyons D, Huntley J, Fierer N, Owens SM, Betley J, Fraser L, Bauer M, Gormley N, Gilbert JA, Smith G, Knight R. 2012. Ultra-high-throughput microbial community analysis on the Illumina HiSeq and MiSeq platforms. *ISME J* 6:1621–1624. <https://doi.org/10.1038/ismej.2012.8>.
 41. Amir A, McDonald D, Navas-Molina JA, Kopylova E, Morton JT, Zech Xu Z, Kightley EP, Thompson LR, Hyde ER, Gonzalez A, Knight R. 2017. Deblur rapidly resolves single-nucleotide community sequence patterns. *mSystems* 2. <https://doi.org/10.1128/mSystems.00191-16>.
 42. McDonald D, Clemente JC, Kuczynski J, Rideout JR, Stombaugh J, Wendel D, Wilke A, Huse S, Hufnagle J, Meyer F, Knight R, Caporaso JG. 2012. The Biological Observation Matrix (BIOM) format or: how I learned to stop worrying and love the ome-ome. *Gigascience* 1:7. <https://doi.org/10.1186/2047-217X-1-7>.
 43. Caporaso JG, Kuczynski J, Stombaugh J, Bittinger K, Bushman FD, Costello EK, Fierer N, Peña AG, Goodrich JK, Gordon JI, Huttley GA, Kelley ST, Knights D, Koenig JE, Ley RE, Lozupone CA, McDonald D, Muegge BD, Pirrung M, Reeder J, Sevinsky JR, Turnbaugh PJ, Walters WA, Widmann J, Yatsunenko T, Zaneveld J, Knight R. 2010. QIIME allows analysis of high-throughput community sequencing data. *Nat Methods* 7:335–336. <https://doi.org/10.1038/nmeth.f.303>.
 44. Weiss S, Xu ZZ, Peddada S, Amir A, Bittinger K, Gonzalez A, Lozupone C, Zaneveld JR, Vázquez-Baeza Y, Birmingham A, Hyde ER, Knight R. 2017. Normalization and microbial differential abundance strategies depend upon data characteristics. *Microbiome* 5:27. <https://doi.org/10.1186/s40168-017-0237-y>.
 45. Mirarab S, Nguyen N, Warnow T. 2011. SEPP: SATé-enabled phylogenetic placement. *Pac Symp Biocomput* 2012:246–258.